

ORIGINAL ARTICLE

Single-Cell RNA Sequencing Reveals the Developmental Landscape of Wheat Roots

Zhenzhen Du¹ | Bin Zhang¹ | Han Weng¹ | Li Gao^{1,2} 

¹State Key Laboratory for Biology of Plant Disease and Insect Pests, Institute of Plant Protection, Chinese Academy of Agricultural Sciences, Beijing, People's Republic of China | ²Institute of Plant Protection, Xinjiang Academy of Agricultural Sciences, Key Laboratory of Integrated Pest Management on Crop in Northwestern Oasis, Ministry of China, Scientific Observing and Experimental Station of Korla, Ministry of Agriculture, Urumqi, Xinjiang, People's Republic of China

Correspondence: Li Gao (xiaogaosx@hotmail.com)

Received: 5 August 2024 | **Revised:** 20 November 2024 | **Accepted:** 26 November 2024

Funding: This work was supported by Xinjiang Major Science and Technology projects (Research, development, and demonstration of key technologies for the green control of major pests on special and superiority crops in Xinjiang, 2023A02009). Li Gao was supported by Xinjiang 2+5 Key Talent Plan Project.

Keywords: allohexaploid wheat | root | scRNA-seq | transcriptional landscape

ABSTRACT

Allohexaploid wheat (*Triticum aestivum* L.) is one of the major crops worldwide, however there is very limited research on the transcriptional programmes of underlying cell type specification. Single-cell RNA sequencing (scRNA-seq) was used to unravel the transcriptome heterogeneity of cells and the composition of cell types in broad-spectrum organisms. Here, we reported the scRNA-seq transcriptomes of single cells from root tips of the wheat Chinese spring (CS) cultivar, defined cell-type-specific marker genes, and identified most of the major cell types. We further profiled the reconstructed developmental trajectories of the stem cell niche (SCN), proximal meristems and meristems, unveiled gene expression signature of water transportation, divulged cell-type-specific asymmetric gene transcription in subgenomes and explored the evolutionary conservation and divergence of wheat cultivar (CS) and rice cultivar (Nip and 93-11, ZH11) cell types through interspecies comparison. Collectively, this work underscored the transcriptional landscape of wheat cultivar (CS) roots and provided a single-cell perspective for differentiation trajectory application, unbalanced gene expression pattern and characteristics of cell types between two plant species, contributing to a better understanding of wheat cultivar (CS) root development at unprecedented resolution.

1 | Introduction

Wheat (*Triticum aestivum* L.) is one of the major crops worldwide, with the largest cultivated area and the widest distribution, providing approximately 20% of daily calories and protein for humans (Tadesse et al. 2019). Roots are important organs for water and nutrient uptake, so intensive research is crucial to gain insight into their developmental landscape and differentiation trajectories (Oh et al. 2017). Li et al. (2019) reported that the root of wheat consists of meristematic zone, elongation zone and maturation zone. Quantifying gene expression in single cells or cell types is

significant for understanding the complex gene regulatory networks involved in wheat root development.

The single-cell sequencing (scRNA-seq) technique makes it possible to mine cell heterogeneity between cell types and within cells in a broad spectrum of organisms, including plant tissues such as in the root of *Arabidopsis* (Efroni and Birnbaum 2016). Recently, in the analysis of the corresponding dynamic profiles of cellular development, scRNA-seq has made great progress in *Arabidopsis*, such as the developmental landscape of the root tips (Denyer et al. 2019; Jean-Baptiste et al. 2019; Ryu et al. 2019; Shulse et al. 2019; Zhang

et al. 2019; Rich-Griffin et al. 2020), vegetative shoot apex (Zhang, Chen, and Wang 2021), stomatal lineage cell (Liu et al. 2020). In plant fields, scRNA-seq was also successfully applied for single-cell transcriptome analysis of rice root tips (Liu et al. 2021; Zhang, Chen, and Wang 2021), rice leaf and root (Wang et al. 2021), rice floret and inflorescence meristems (Zong et al. 2022), maize root (Li et al. 2022; Ortiz-Ramírez et al. 2021), maize shoot stem-cell niche (Satterlee, Strable, and Scanlon 2020) and maize anthers (Nelms and Walbot 2019). Regarding allohexaploid bread wheat, transcriptional landscape and asymmetric gene transcription of root tips in AiKang58 (AK58) cultivar were revealed by another different technology—single nuclei RNA sequencing (snRNA-seq) (Zhang et al. 2023). However, we focused on the research of whole protoplast cells and captured more wheat (CS) root tip cells using the scRNA-seq platform.

scRNA-seq obtains not only gene transcripts in the nucleus, but also in the cytoplasm, allowing for a more comprehensive interpretation of gene expression during root tip development at the gene level. Here, through scRNA-seq we successfully investigated the gene expression of 13063 captured and sequenced single cells. Together with computer analysis and *in situ* hybridization results, we identified most major cell types with cell-type-specific marker genes. Moreover, we revealed the cellular heterogeneity of wheat root tips and clarified the molecular mechanisms of water transportation with *AQPs*. Asymmetric transcription of subgenomes in different cell types, as well as conserved and divergent gene expression patterns of root tip tissues between wheat and rice species were also analysed. The results of this study unravelled the developmental landscape of wheat root tips, which opening new avenues to root developmental research at single-cell resolution.

2 | Results

2.1 | ScRNA-seq in Wheat (CS) Roots

We selected the allohexaploid wheat cultivar (CS) with sequenced genome (<https://wheat-urgi.versailles.inra.fr/Seq-Repository>) (V 2.1) and performed scRNA-seq by collecting 40 root tips (1 cm in length) of 4-day-old seedlings. Isolated protoplasts for scRNA-seq were loaded on a commercial 10 × Chromium platform (10 × Genomics) (Figure S1a). Subsequently, libraries were constructed, and high throughput sequencing was performed (Illumina HiSeq2000 sequencer, Shanghai OE Biotech, China) (Figure S1b). One cell type was formed by clustered cells showing similar gene expression profiles. The results of dimensionality reduction based on principal component analysis (PCA) were visualized by the t-distributed stochastic neighbor embedding (*t*-SNE) tool. The clustering algorithm was adopted shared nearest neighbor clustering (SNN) to obtain the optimal cell clusters with unsupervised method (Figure S1b). We also employed uniform manifold approximation and 86 projection (UMAP) algorithm to visualize the clustering result (Figure S1c), but found that *t*-SNE was more ideal. Data were prefiltered at both cell and gene level by fitting the generalized linear model (Figure S2a) and the distribution of nGene (Figure S2b,c) and nUMI (Figure S2d,e). The percentage of mitochondrial (median < 0.016%) and chloroplast (median < 0.017%) genes showed that the impact of

mitochondrial and chloroplast genes on clustering was minor (Figure S2f). After quality control, we successfully captured 13063 wheat (CS) root cells with 2523 mean unique molecular identifiers (UMIs), 43 417 mean reads and 1851 median genes per cell (Table S1). Therefore, we obtained high-quality cells to ensure the reliability of scRNA-seq data sets. The results in Figure 1a showed that root cells were grouped into 19 clusters and they were annotated as 12 cell types. A schematic of the root tip structure was depicted to mimic the de facto developmental map of wheat (CS) root (Figure 1b). Through the analysis of differentially expressed genes (DEGs) and the identification algorithm of cell markers among the clusters, we obtained cluster-enriched genes and the top 10 cluster-specific markers for each cluster (Table S2).

2.2 | Identification of Cell Type Clusters in Wheat (CS) Roots

The produced 12 cell types (Figure 1a) were annotated as following steps. First, we blasted homologous cluster-specific markers of wheat (CS) (Table S2) with other cultivar and species in root tips, such as wheat (AK58) (Zhang et al. 2023), maize (Li et al. 2022), rice (Zhang, Chen, and Wang 2021; Liu et al. 2021) and *Arabidopsis* (Denyer et al. 2019; Jean-Baptiste et al. 2019; Ryu et al. 2019; Shulse et al. 2019; Zhang et al. 2019; Rich-Griffin et al. 2020), and examined their expression patterns. We obtained 69 homologous marker genes in total, and in list of top 10 markers of CS for annotation, they were *histone H2A.2.2* (*TaH2A.2.2*) highly and specifically expressed in meristem, *blue copper protein* (*TaBCP*), *uclacyanin-3-like* (*TaUCC3L*), *Laccase 3* (*TaLAC3*) and *Casparian strip membrane protein 1* (*TaCASP1*) in endodermis, *cellulose synthase A catalytic subunit 9* (*TaCesA9*) and cysteine protease *XCP1-like* (*TaXCP1L*) in xylem (Figure 1c; Table S3; marked with an asterisk). Notably, except *TaH2A.2.2*, *TaCesA9* and *TaPRPDC2.15*, most homologous markers (Table S4) were from the report of Zhang et al. (2023), which were generated by alignment of the top 100 cell-type-specific markers in CS and AK58. We presented the shared and CS-dependent markers (Table S4) which indicated the production of novel markers in our study. We also summarized homologous genes with well-studied biological functions and expression patterns not involved in root tips reports by scRNA-seq (Table S3; Figure 1c). Meanwhile, the results of GO enrichment for each cluster (Table S5) were also helpful for several cluster annotations. Furthermore, we conducted *in situ* hybridization assays for almost 50 cluster-specific markers and only 9 of them showed specific expression accordingly (Figure 1d), enabling us to validate our annotation and identify unassigned clusters faithfully.

Cluster 9 was assigned to the SCN, and Clusters 7 and 12 were assigned to the proximal meristem and meristem, respectively. The results of *in situ* hybridization showed that the specific marker gene of *TraesCS2B03G0976900* in Cluster 9 was highly expressed in the SCN (Figure 1d). In *Arabidopsis*, a high concentration of superoxide anion (O_2^-) in the central zone (CZ) of shoot stem cells can activate the expression of the *WUS* (*WUSCHEL*) to maintain stem cell fate (Zeng et al. 2017) and prevent cells from proliferating to differentiation (Tsukagoshi, Busch, and Benfey 2010). In living cells, two primary sources for producing O_2^- are NADH dehydrogenase of mitochondrial complex I in the respiratory chain and NADPH oxidase in the plasma membrane

(Malinska et al. 2012; Hamanaka et al. 2013). Genes related to mitochondrial respiratory chain complex I (CI), NAD(P)H activity, NADP⁺ activity, and hydrogen peroxide (H₂O₂) catabolic process were highly and specifically enriched in Cluster 9 (Table S5). Therefore, Cluster 9 was annotated as SCN. Markers *TraesCS3B03G1129700* and *TaH3.2* of Clusters 7 and 12,

respectively, exhibited specific signals in the proximal meristem and meristem according to *in situ* hybridization (Figure 1d). In the top 10 cluster-specific markers of Clusters 7 and 12, genes of several ribosomal proteins (*TaRpl10a-1*, *TaRplS27aL*, *TaRpl10a-1*, *TaRpl10a-1L*) and histones (*TaH2B.2L*, *TaH4*, *TaH3.2*, *TaH2A.2.1*, *TaH2A.2.2*) were prominently listed (Figure 1c).

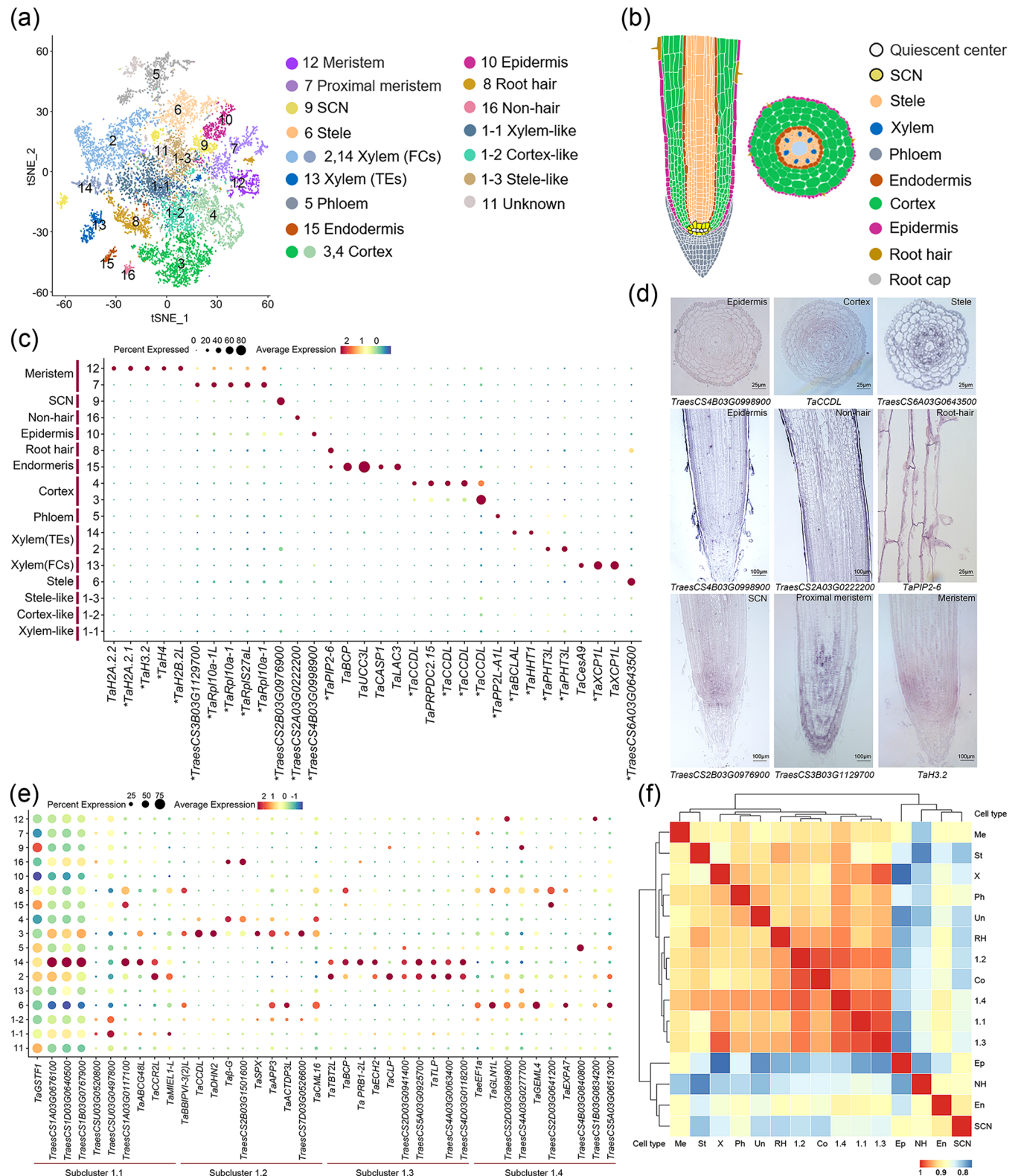


FIGURE 1 | Legend on next page.

which were closely related to cell division. The expression patterns of genes associated with histones, mainly and predominantly transcribed in Cluster 12 were also showed in t-SNE plot (Figure S3). Genes regulating ribosomal large subunit assembly and translation, nucleosome assembly and translation were also highly enriched in Clusters 7 and 12, respectively (Table S5). Therefore, Clusters 7 and 12 were annotated as proximal meristem and meristem, accordingly.

Cluster 10, Cluster 16 and Cluster 8 were identified as epidermis, non-hair and root hair, respectively. In situ hybridization suggested that marker genes *TraesCS4B03G0998900*, *TraesCS2A03G0222200* and *TaPIP2-6* of Clusters 10, 16 and 8 were specifically expressed in the epidermis, non-hair and root hair, respectively (Figure 1d). Correspondingly, the GO annotation analysis showed that genes of water channel activity were highly enriched in Clusters 8 and 16 (Table S5), which was inseparable from the function of water absorption.

Cluster 15 was annotated as endodermis. *TaBCP*, *TaUCC3L*, *TaLAC3* and *TaCASP1* were cell-type specific markers of Cluster 15 in CS and endodermis in AK58 (Zhang et al. 2023) (Tables S3 and S4). Additionally, *TaBCP* and *TaUCC3L* were two homologous genes of *UCC1* and *UCC2* (*uclacyanin proteins*) of *Arabidopsis*, and *UCC1* and *UCC2* were involved in the formation of lignified nanodomains within casparyan strip (Reyt et al. 2020). *LAC3*-based extracellular domain and casparyan strip membrane domain (CSDM) in *Arabidopsis* could provide precise bidirectional lignification location information for casparyan stripformation (Zhuang et al. 2020). The formation of casparyan strip in *Arabidopsis* also requires cooperation by localized NADPH oxidase, peroxidases and the action of *CASPs* (Lee et al. 2013). Genes related to NAD(P)H activity were highly enriched in Cluster 15 (Table S5).

Clusters 3 and 4 were designated as the cortex. There were one and three genes of *TaCCDL* encoding *cortical cell-delineating protein-like protein* highly expressed in Clusters 3 and 4 (Figure 1c), respectively. In situ hybridization confirmed the abundant transcript of *TaCCDL* (*TraesCS1B03G0645800*) in the cortex (Figure 1d). In soybean, a proline-rich 14 kDa protein was located in the cortex of the root tip (Choi et al. 1996). In Cluster 4, the expression level of its homologous protein, *14 kDa proline-rich protein DC2.15-like* (*TaPRPDC2.15*) was also significantly higher (Figure 1c).

Cluster 5 was annotated as phloem. In this cluster, *PHLOEM PROTEIN 2-LIKE A1-like* (*TaPP2L-A1L*), the homologous gene of

AtPP2-A1 which was specifically expressed in the companion cell-sieve element complex of *Arabidopsis* (Beneteau et al. 2010; Dinant et al. 2003), was specifically and highly expressed (Figure 1c). The xylem includes several cell types, such as fibre cells (FCs), xylem parenchyma cells and tracheary elements (TEs), which contain vessel cells and tracheids (Ohashi-Ito and Fukuda 2014). Clusters 13 were assigned as TEs of xylem, and Clusters 2 and 14 were assigned as FCs of xylem. *TaCesA9* and *TaXCP1L* were preferentially expressed in Cluster 13 of CS (Figure 1c) and xylem of AK58 (Zhang et al. 2023) (Tables S3 and S4). Furthermore, *AtXCP1* in *Arabidopsis* are specifically expressed in TEs (Funk et al. 2002; Avci et al. 2008; Yamaguchi et al. 2011). *TaCesA9* was a homologous of *OsCesA9* which was involved in synthesis in the secondary wall in rice (Tanaka et al. 2003; Wang et al. 2012) and TEs of xylem possesses secondary wall thickenings in *Arabidopsis* (Schneider et al. 2017). TEs play a pivotal role in water transporting (Turner, Gallois, and Brown 2007), and genes involved in water channel activity were highly enriched in Cluster 13 correspondingly (Table S5). Therefore, we annotated Cluster 13 as TEs of xylem. Genes of putrescine *hydroxycinnamoyltransferase 3-like* (*TaPHT3L*) and *Omega-hydroxypalmitate O-feruloyl transferase* (*TaHHT1*), *benzoate-CoA ligase, peroxisomal-like* (*TaBCLAL*) related to the lignin monomer biosynthesis process were highly expressed in Clusters 2 and 14, respectively (Figure 1c). Meanwhile, GO terms related to phenylalanine ammonia-lyase activity (Yamada et al. 1981), hydroxycinnamoyltransferase activity (Wang et al. 2015), and 4-coumarate-CoA ligase activity (Barros et al. 2015) were enriched in Cluster 2 (Table S5). GO enrichment of the process of lignin biosynthesis, such as cinnamic acid biosynthetic process (Hoskins 1984), L-phenylalanine catabolic process (Yamada et al. 1981) were shown in Clusters 2 and 14. According to Li et al. (2021), Clusters 2 and 14 belong to TEs or FCs, and Cluster 13 was already annotated as TEs, so Clusters 2 and 14 were assigned FCs of the xylem. Clusters 6 were annotated as a stele, because *TraesCS6A03G0643500* was specifically detected in immature sieve elements of AK58 (Zhang et al. 2023) (Tables S3 and S4), and specific markers *TraesCS6A03G0643500* were also expressed in the stele cells of CS (Figures 1c,d).

Because the markers in Cluster 1 were not specific enough for annotation, we conducted subcluster analysis and found that it can be divided into four subclusters (Figure S4a) and the proportion of four subclusters were given (Figure S4b). Based on the top 10 cluster-specific markers of four subclusters (Figure 1e), we found that the top 10 markers of Subclusters 1.1 and 1.3 were highly expressed in Clusters 2 and 14 of xylem. GO enrichment terms related to the lignin metabolic process were

FIGURE 1 | scRNA-seq and cell type annotation of wheat (CS) root tips. (a) t-SNE visualization of putative 19 clusters and 12 cell types from 13 063 cells and their spatial distribution in wheat (CS) root tips. SCN: stem cell niche; xylem (TEs): tracheary elements of xylem; Xylem (FCs): fibre cells of xylem. Each dot indicates a single cell. (b) A schematic of the wheat (CS) root tip structure. Colours in the diagram of the root tips indicate corresponding cell clusters. The grayish white and black parts indicate uncaptured cells. (c) Dotplot showing the expression of cell-type-specific marker genes. Genes marked with asterisks were novel markers produced in this study. Genes with the same name were listed according to the order in Table S3. Dot size indicates the expression percentage of a given gene in cluster cells, and dot colour indicates the expression level of a given gene in distinct cell clusters. (d) RNA in situ hybridization validation of cluster-specific markers. (e) Dotplot showing the expression of marker genes in four subclusters of Cluster 1. Dot size indicates the expression percentage of a given gene in cluster cells, and dot colour indicates the expression level of a given gene in distinct cell clusters. (f) Heatmap showing Pearson's correlation of cell subclusters in Cluster 1 with other cell types. Co: cortex; En: endodermis; Ep: epidermis; RH: root hair; St: stele; X: xylem; Ms: meristem; NH: non-hair; P: phloem; SCN: stem cell niche. The color bar indicates the correlation coefficient.

enriched in clusters 1.1, and cinnamic acid biosynthetic process (Hoskins 1984), L-phenylalanine catabolic process (Yamada et al. 1981) were enriched in clusters 1.1 and 1.3. Meanwhile, the top 10 markers of subcluster 1.2 and 1.4 were highly expressed in Cluster 3 of cortex, and Cluster 6 of stele, accordingly. High correlation of subclusters 1.1 and 1.3 (labelled as Cluster 1-1) with the xylem, subcluster 1.2 (labelled as Cluster 1-2) with cortex and Subcluster 1.4 (labelled as Cluster 1-3) with stele were revealed by heatmap (Figure 1f). Therefore, we assigned Clusters 1-1, 1-2 and 1-3 into xylem-like, cortex-like and stele-like, respectively. Due to the lack of specific marker information, we assigned Cluster 11 as unknown. Additionally, we depicted the expression patterns of other top 10 cluster-specific marker genes produced in this study (Figure S5). In conclusion, we identified most of the major cell types in wheat (CS) roots, indicating that the construction of a single-cell library was successful.

2.3 | Differentiation Trajectory Reconstruction of SCN and Meristem Cells

The capture of terminal and intermediate states of cells during the dynamics of differentiation provides a completely new vision for understanding cellular developmental progress. To reveal the continuous biological process behind the SCN (Cluster 9), proximal meristem (Cluster 7) and meristem (Cluster 12), we applied monocle 2 for differentiation trajectory reconstruction of three cell populations. The successive pseudotime order is shown in Figure 2a. Cells from Cluster 9 were at the beginning of inferred trajectories, then Clusters 7 and 12 were ordered at two distinct branches bifurcated (Figure 2b). Expression of cell type markers on the trajectory indicates the high transcription of *TraesCS2B03G0976900* at the pre-branch and gradually weakened signals with the development of pseudotime. While *TraesCS3B03G1129700* and *TaH3.2* were observed in the lineages of proximal meristem and meristem tissues, respectively (Figure 2c-e).

Highly variable genes based on average expression level were divided into four modules (Figure 2f). In pre-branch, we first focused on the expression of important genes. The accumulation of auxin concentration gradients plays an important role in SCN maintenance in *Arabidopsis*. Auxin perception relies on the signal perception module of the SCFTIR1/AFBs-AUX/IAA-ARF complex, thereby regulating the transcription of auxin-responsive genes (Mockaitis and Estelle 2008; Dubey et al. 2021). In module 1 of pre-branch, genes encoding auxin-responsive proteins were highly expressed, such as *auxin-responsive protein 1* (*TaIAA1*), *auxin-responsive protein 5-like* (*TaIAA5L*), *auxin-responsive protein 19-like* (*TaIAA19L*), *probable auxin efflux carrier component 5B* (*TaPIN5b*) and *auxin response factor 5-like* (*TaARF5L*). Then, GO enrichment showed that genes associated with the aromatic amino acid family catabolic process was enriched in module 1 (Figure 2f), which may be similar to the gene activation of *PLT2* in the quiescent center (QC) of *Arabidopsis* (Santuari et al. 2016). Meanwhile, positive regulation of auxin metabolic process, positive regulation of auxin biosynthetic process, auxin influx and auxin efflux were also enriched in pre-branch. For SCN function, an auxin maxima at QC and its cells beneath is critical. In branch 1, we

found that the tryptophan metabolic process pathway related to the activation of *PLT2* in QC (Santuari et al. 2016) was shown in module 3, and regulation of the auxin-mediated signalling pathway, the ethylene-activated signalling pathway related to QC regulation (Ortega-Martinez et al. 2007) were also highly enriched (Figure 2f). They revealed the existence of transitional state cells from SCN to proximal meristem. GO enrichment of module 4 demonstrated that genes related to translation, ribosomal small/large subunit assembly and ribosomal large subunit biogenesis were highly enriched (Figure 2f), indicating that proximal meristem cells were undergoing cell division. In branch 2, cells in module 2 also demonstrated gene signatures of cell division in meristem because nucleosome assembly, chromatin organization, and chromosome condensation were highly enriched (Figure 2f). Thus, gradual transitions from cells in SCN (Cluster 9) to proximal meristem (Cluster 7) or meristem (Cluster 12) were achieved in our survey, implying the accuracy of cell type annotation and achievable potential analyses with the atlas. More importantly, scRNA-seq can recapitulate the cell differentiation trajectory for the SCN (Cluster 9) to proximal meristem (Cluster 7) or meristem (Cluster 12), and depicted the temporal expression changes of highly variable genes in the dynamic process. In parallel, we also performed slingshot analysis of three cell clusters, which showed the same developmental differentiation trajectory of the three cell populations, and confirmed the analysis results of monocle 2 (Figure S6).

2.4 | Water Transportation Patterns Across Wheat Root Cell Types

AQPs (aquaporin) are of great significance in water transportation. Madrid-Espinoza et al. (2018) identified a total of 113 AQPs based on the wheat genome sequence, and 22 AQPs expressions of genes were detected in this study (Table S6; Figures 3a-3d). To explore how AQPs work in wheat (CS) root tips, we pooled genes related to *plasma membrane intrinsic protein (PIP)*, *tonoplast intrinsic protein (TIP)*, *nodulin 26-like membrane intrinsic protein (NIP)* and plotted their expression patterns (Table S6; Figure 3a-d). *OsPIP2;1* of rice, *ZmPIP2;1* of maize and coexpression of *HvPIP2;1* and *HvPIP1;2* were reported to increase the water permeability to enhance water transportation (Ding et al. 2019; Fetter et al. 2004; Horie et al. 2011). Typically, coexpression with *AtPIP2;1* and *AtPIP1;2*, *AtPIP1;5* further increased water permeability, which cannot work when expressed alone (Byrt et al. 2017). Based on Figure 3a, we noted that in cortex (Clusters 3 and 4), root hair (Cluster 8) and non-hair (Cluster 16) cells, three *TaPIP1;2* and two *TaPIP1;5L* genes were highly expressed. Except for root hairs, another two *TaPIP2;1* genes were detected in the cell types mentioned above (Figure 3b). We also observed high levels of transcripts for another four *TaPIP1;5* genes in root hair (Cluster 8) and non-hair (Cluster 16) cells (Figure 3b). Thus, the cortex and non-hair shared common water transportation pathways facilitated by the cooperation of *TaPIP1;2*, *TaPIP1;5* with *TaPIP2;1*, and root hairs were not included due to the lack of *TaPIP2;1*. As shown in Figure 3a,b, in the TEs of xylem (Cluster 13), three genes related to *TaPIP1;2* and two genes related to *TaPIP2;1* were highly and specifically expressed, indicating that cooperation of *TaPIP2;1* and *TaPIP1;2* was the

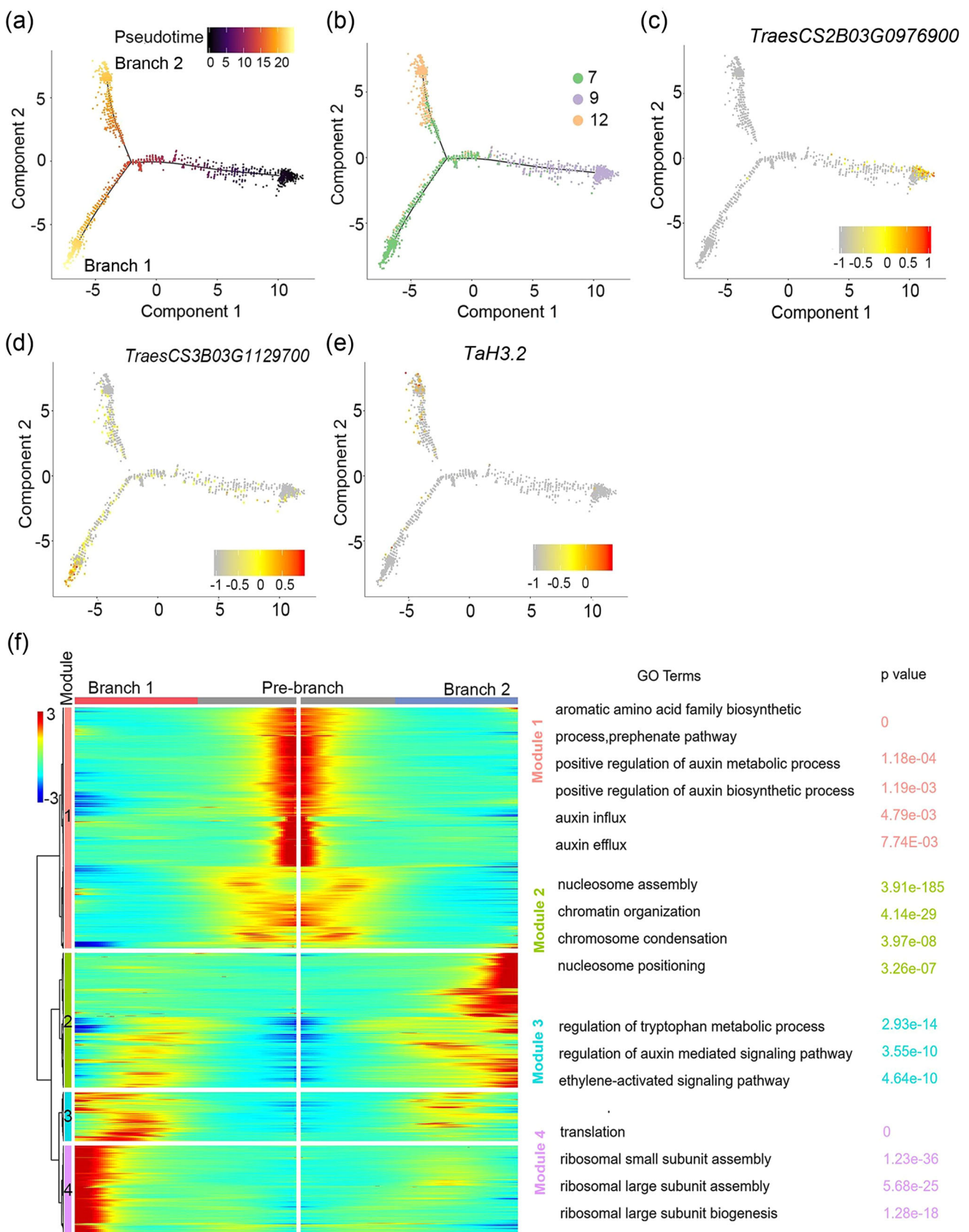


FIGURE 2 | Differentiation trajectory of SCN, proximal meristem and meristem by pseudotime analysis. (a) Pseudotime reconstruction of SCN, proximal meristem and meristem by monocle 2. Colours indicate different pseudotime scores. (b) Cell types presented on the differentiation trajectory. (c–e) Expression of cluster-specific marker genes across the pseudotime trajectory. The colours represent the expression levels of these genes in individual cells. (f) Heatmap showing the expression of highly variable genes and GO enrichment analysis of each module across the pseudotime. *p* values of GO enrichment were given. [Color figure can be viewed at wileyonlinelibrary.com]

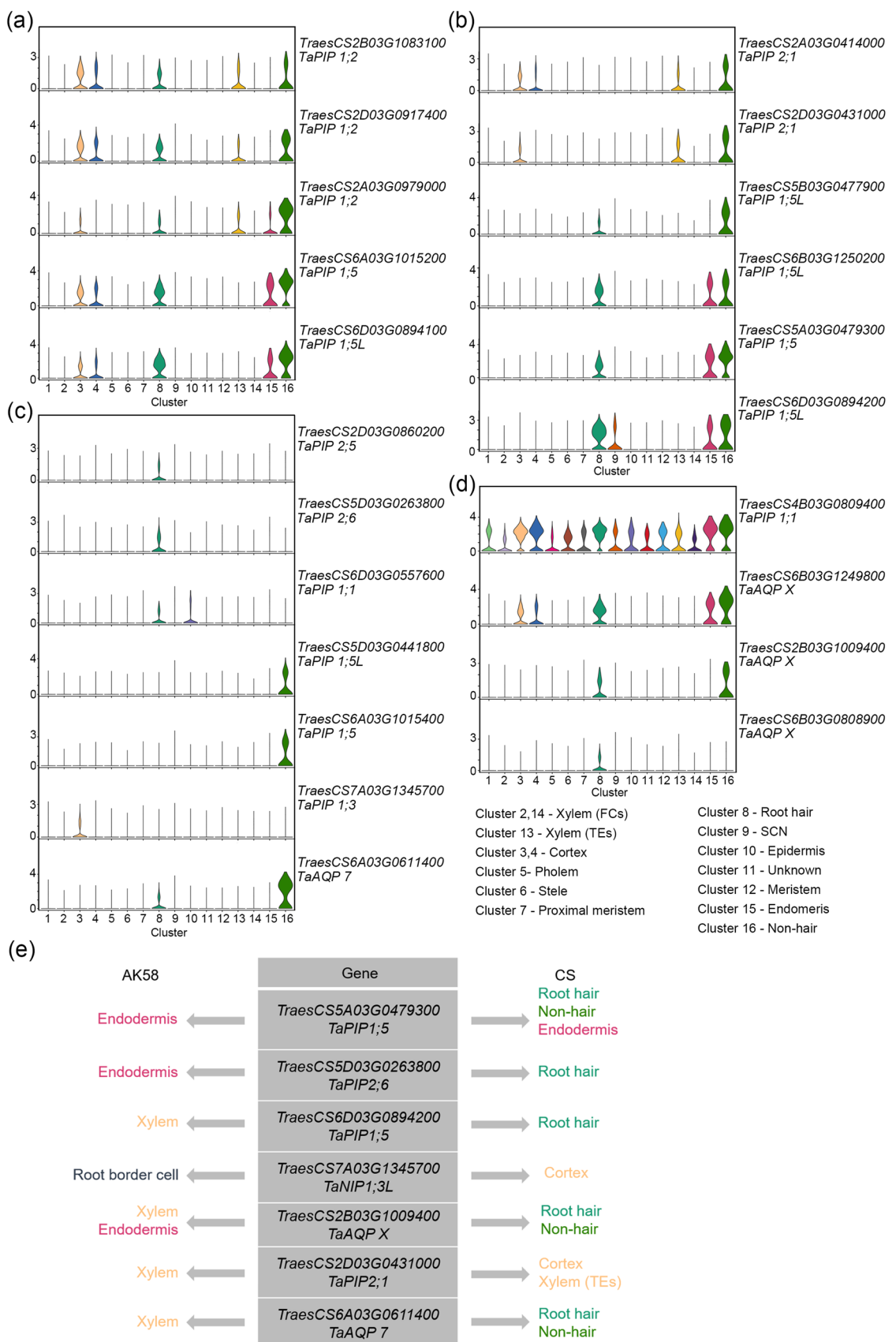


FIGURE 3 | Expression patterns of genes involved in water transportation. (a-d) Expression patterns of AQPs genes displayed by violin plots. The length of the violin plot represents the gene expression level, and the width represents the proportion of cells expressing different AQPs genes (y-axis) across each cluster (x-axis). (e) Shared genes of AQPs expressed in both root tips of CS and AK58. The arrows on both sides indicated the tissues in which genes were expressed in two cultivars. [Color figure can be viewed at wileyonlinelibrary.com]

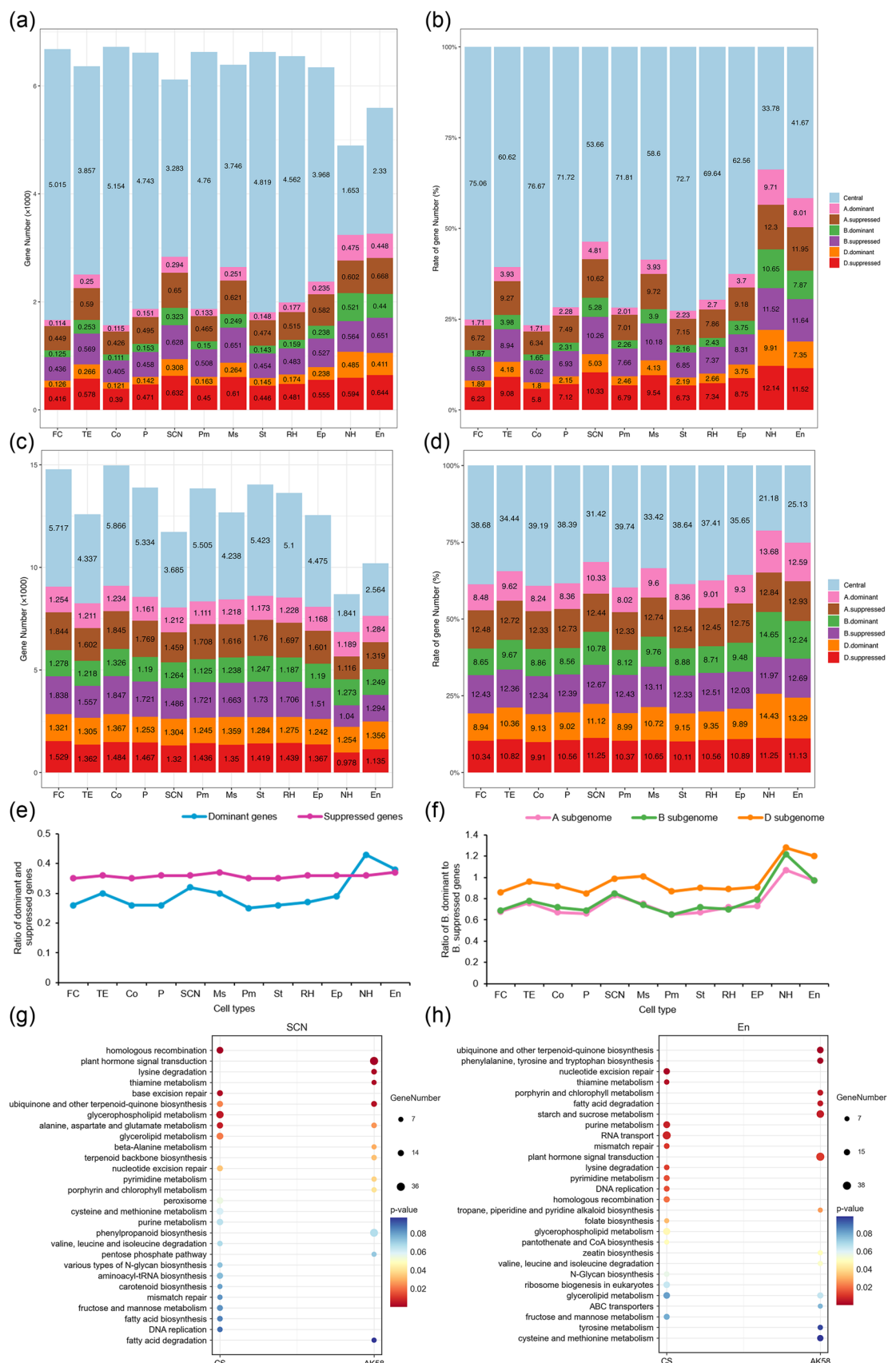


FIGURE 4 | Legend on next page.

only one way to promote water transportation. In the endodermis (Cluster 15), *TaPIP1;2* and five *TaPIP1;5* genes were highly expressed, but *TaPIP2;1*, a cooperator of *TaPIP1;5*, was not detected. Therefore, the mechanism of promoting water transportation through AQPs in TEs and endodermis was accordingly cooperation of *TaPIP2;1*, *TaPIP1;2* and *TaTIP1;1* water channels, which were relatively simple compared with other tissues. In addition, one *TaPIP1* gene was highly expressed in SCN (Cluster 9) (Figure 3b), but *TaPIP1;5* may not work independently, like *AtPIP1;5* (Byrt et al. 2017).

In maize and *Arabidopsis*, the coexpression of *ZmPIP1;2* and *ZmPIP2;5* and *AtPIP2;6* independently resulted in an increase in the water permeability coefficient (Fetter et al. 2004). In Figure 3c, in root hair cells (Cluster 8) and non-hair (Cluster 16), genes of *TaPIP2;5*, *TaPIP2;6*, and two *TaPIP1;5* transcripts showed specific expression, respectively; one *TaPIP1;1* gene was detected in root hair cell and epidermis (Cluster 10). Moreover, *TaNIP1;3L* were predominantly expressed in the cortex (Cluster 3), and *TaAQP;7* in root hair and non-hair cells, respectively (Figure 3c). Thus, root hairs of wheat exhibited a unique channel of *TaTIP1;1*, *TaPIP2;6*, and coexpression of *TaPIP1;2* and *TaPIP2;5* to increase the uptake of water. In addition, unique channel also existed in the cell type of cortex (*NIP1;3L*), epidermis (*TaTIP1;1*, *TraesCS6D03G557600*), root hair (*TaAQP;7*) and non-hair cells (*TaAQP;7*) (Figure 3c). In Figure 3d, another *TaPIP1;1* (*TraesCS4B03G0809400*) gene was expressed in all cell types without specificity. Three AQPs were not divided into subfamilies, so we named them *TaAQP X* (Figure 3d). Furthermore, the expression patterns of genes associated with the response to water deprivation and water channel activity revealed that these genes were distributed mainly in the cortex, endodermis, xylem TE, root hair and non-hair cells (Figure 3a-d), which was inextricably linked to the existence of AQPs.

By comparing with the top 100 cell-type specific markers identified by Zhang et al. (2023), we found that 7 shared genes of AQP expressed in both root tips of CS and AK58 (Figure 3e). For example, *TaPIP1;5* was highly transcribed in the endodermis of two cultivars, and *TaPIP2;1* in the root hair. While transcription of other five aquaporins were showed in different tissues of two cultivars, such as *PIP2;6* was detected in the root hairs CS and endodermis of AK58. In summary, scRNA-seq allowed us to dissect the distinct distribution patterns of water transportation for further study of possible multiplicate regulatory programmes across cell tissues.

FIGURE 4 | Asymmetric gene transcription based on scRNA-seq in root cell types of wheat (CS). (a, b) The asymmetric expression of the triad in the central part of Figure S7 observed in all clusters. The gene number (a) and rate of gene number (b) were given, respectively. A. dominant indicates that in A subgenome, gene expression is higher than the homoeologs of B and D subgenomes; A. suppressed indicates that in A subgenome, gene expression is lower than the homoeologs of B and D subgenomes. Balance indicates the expression of homoeologs from A, B and D subgenomes are similar. FC: Fibre cells of xylem; TE: tracheary elements of xylem; Co: cortex; P: phloem; SCN: stem cell niche; Pm: proximal meristem; Ms: meristem; St: stele; RH: root hair; Ep: epidermis; NH: non-hair; En: endodermis. (c, d) The asymmetric expression of all triads observed in all clusters. The gene number (c) and rate of gene number (d) were given, respectively. (e) The line chart showing the ratio of dominant and suppressed genes in different cell types. The ratio of dominant and suppressed genes showed in different colours. (f) The line chart showing the ratio of dominant to suppressed genes of A subgenome, B. dominant to B. suppressed genes of B subgenome, and D. dominant to D. suppressed genes of D subgenome showed in different colours. (g, h) KEGG analysis of SCN (g) and endodermis (h) in CS and AK58. *p* values were given and the gene number were represented by the size of the filled circles. [Color figure can be viewed at wileyonlinelibrary.com]

2.5 | Cell-Type-Specific Asymmetric Gene Expression in Subgenome of Wheat (CS)

The genome of allohexaploid wheat consists of three subgenomes (A, B and D) in which homoeologs show asymmetric expression (Feldman et al. 2012). Currently, the research on subgenomes asymmetric expression of homoeologs genes is mainly based on a whole organ of mixed cells. We showed the biased pattern of average gene expression of all genes in wheat (CS) root cells (Figure S7; Table S7), and extracted the triads from the central section and observed their unbalanced expression in root cell types (Figure 4a,b; Table S8). Statistics through summation suggested that there were 39.38% genes in TEs were asymmetric transcribed, 46.01% in SCN, 41.4% in the meristem, 66.08% of genes in non-hair, 58.05% of genes in endodermis, and 23.33%–37.44% genes in remaining tissues (Figure 4b; Table S8). Therefore, we can be better to decode the asymmetric expression of genes in wheat (CS) roots at the single-cell level, and scRNA-seq manifested great potential in revealing cell heterogeneity.

We further analyzed the percentage of asymmetric transcription and found the percentage of genes in TEs, SCN, meristem, non-hair, endodermis and remaining tissues were 65.56%, 68.58%, 66.58%, 78.82%, 74.87% and 60.26%–64.35%, accordingly. (Figure 4c,d; Table S9). Notably, in TEs, SCN, meristem, non-hair and endodermis, the percentage of asymmetric transcribed homologous genes were higher than other cell types (Figure 4d), which was mainly attributed to the higher ratio of asymmetric transcription of dominant genes from three subgenomes than other tissues (Figure 4e). Therefore, the asymmetric transcription of homologous genes, especially dominant genes, in the three subgenomes plays a more important role in the formation of TEs, SCN, meristem, non-hair and endodermis tissue. Correspondingly, the ratio of the dominant gene to the suppressed gene was the higher in these tissues, especially in SCN, non-hair and endodermis, they were 0.83, 0.97, 1.07 in subgenome A, 0.85, 0.97, 1.22 in subgenome B, 0.99, 1.20, 1.28 in subgenome D, respectively (Figure 4f). Differentiation trajectory depicted the arise of asymmetric expression transcription followed with the appearance of SCN cells in the pseudotime order (Figure S), and the results of non-hair and endodermis were similar. Furthermore, the minimum ratio of dominant to suppressed gene in A, B and D subgenomes of CS were 0.65, 0.65 and 0.85 (Figure 4f). We conducted KEGG analysis on the dominant genes of SCN and endodermis in wheat (CS and AK58), and found that there were mainly

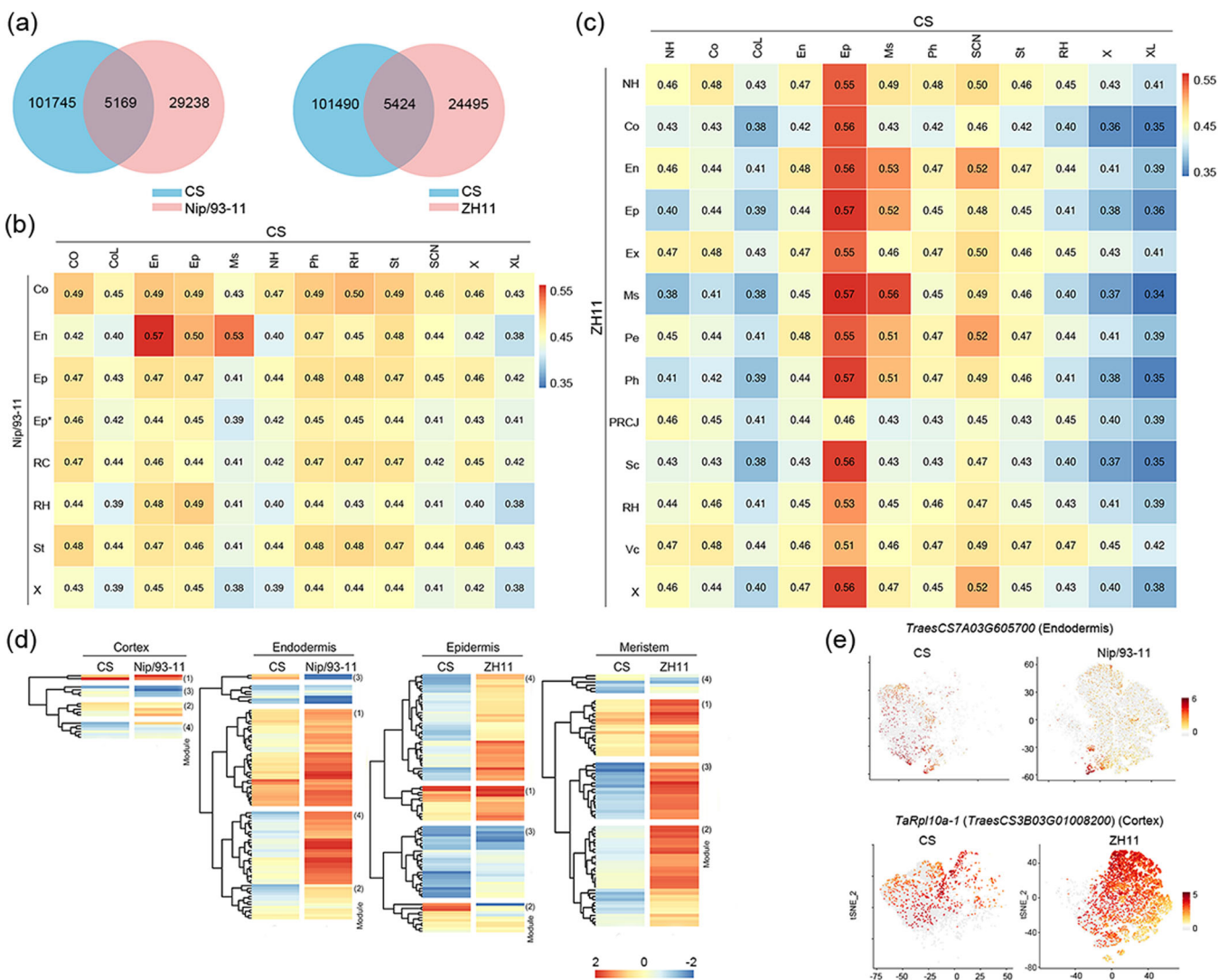


FIGURE 5 | Interspecies comparison of single-cell transcriptomes of wheat (CS) and rice (Nip and 93-11, ZH11) roots. (a) Venn diagram showing the one-to-one homologous gene numbers of wheat (CS) and rice (Nip and 93-11) (a), wheat (CS) and rice (ZH11) (b). (b, c) Heatmap showing the correlation of cell types between wheat (CS) and rice (Nip, 93-11) (c), between wheat (CS) and rice (ZH11) (d). Co: cortex; En: endodermis; Ep: epidermis; Ep*: epidermis (near root hair); RC: root cap; RH: root hair; St: stele; X: xylem; Ms: meristem; NH: non-hair; P: phloem; SCN: stem cell niche; Ex: exodermis; Pe: pericycle, PRJC: putative root cap junction; Sc: sclerenchyma; VC: vascular cylinder. (b, c) We use root hair and non-hair to represent the trichoblast and atrichoblast cell types in ZH11, respectively. Different colours represent different expression levels. (d) Heatmap showing conserved genes in relatively highly correlated cell types of two species. The colour bar shows the scaled expression level. (e) The expression patterns of two shared marker genes in the cortex of wheat (CS) and rice (Nip and 93-11), in the meristem of wheat (CS) and rice (ZH11), respectively. The colour bar shows the scaled expression level. [Color figure can be viewed at wileyonlinelibrary.com]

different terms enriched in both SCN and endodermis tissues between two cultivars (Figure 4g,h). For example, in SCN, homologous recombination, base exception repair, and so forth, were enriched in CS, while in AK58, they were plant hormone signal transformation, lysine degradation, and so forth.

2.6 | Conservation and Divergence of Root Development Between Wheat Cultivar (CS) and Rice Cultivar (Nip and 93-11, ZH11)

Interspecies comparison analysis was conducted to reveal the conservation and divergence of cell types between wheat cultivar (CS) and three different rice cultivars (Nip and 93-11, ZH11) (Liu et al. 2021; Zhang, Chen, and Wang 2021). All cell types of wheat

root, except for clusters of 1-1, 1-2, 1-3, 1-4 and 11, were used for subsequent analysis. Here, 5169 and 5424 one-to-one homologous genes were accordingly obtained and analyzed (Figure 5a). As shown in Figure 5b, the cortex and endodermis tissues of wheat (CS) and rice (Nip and 93-11) were relatively highly correlated, with correlation coefficients of 0.49 and 0.57, respectively. In Figure 5c, relatively high similarity appeared in epidermis and meristem tissues of between wheat (CS) and rice (ZH11), with Pearson's correlation coefficients of 0.57 and 0.56, respectively. In relatively highly correlated cell types, the conserved genes of two species were pooled (Table S10), and their expression patterns were presented in modules 1 and 2 of heatmap showed in Figure 5d, implying the shared cell type markers between the two species. We also obtained species-specific programmes in modules 3 and 4 of the heatmap (Table S10; Figure 5d), suggesting divergent gene expression of

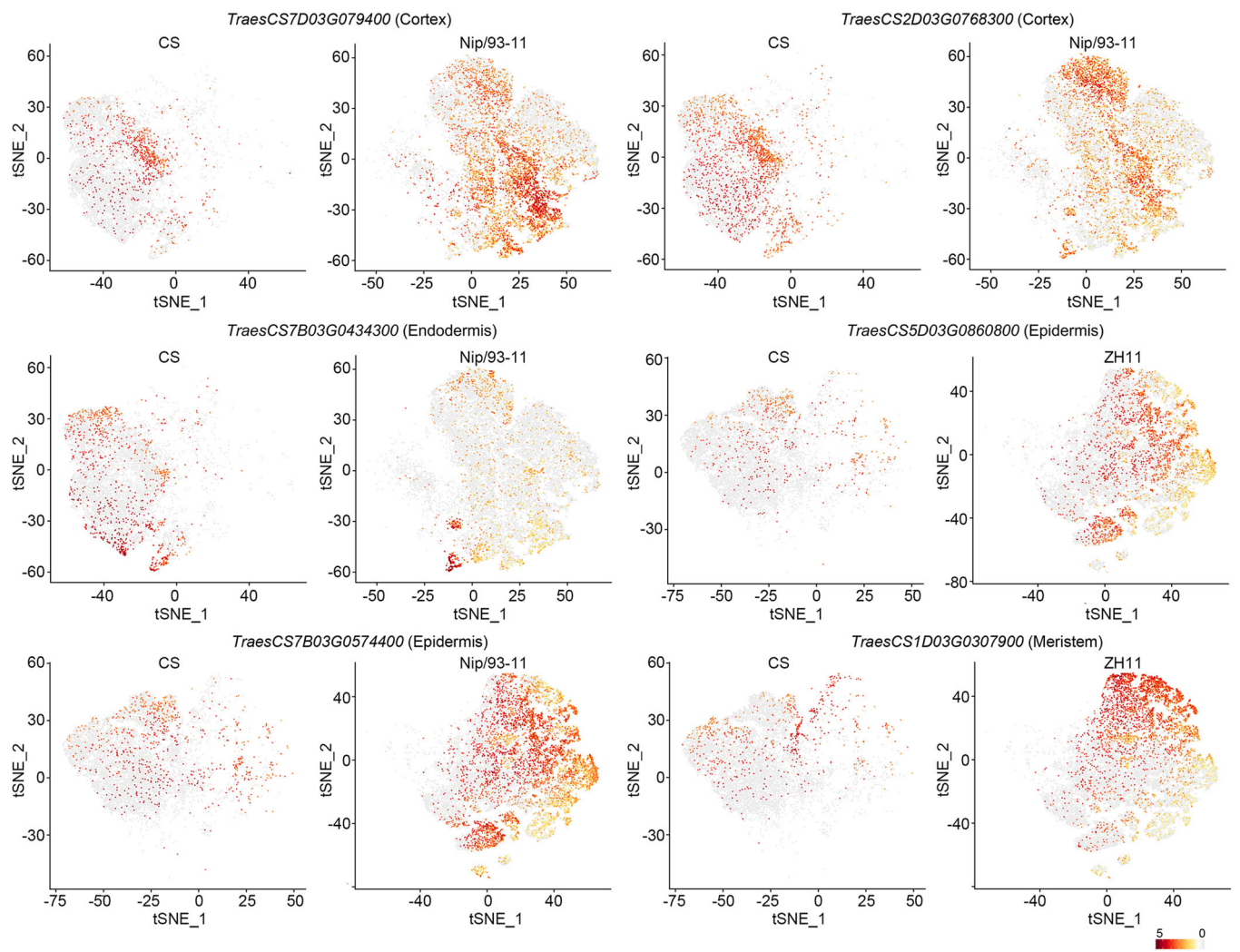


FIGURE 6 | Expression patterns of other six shared marker genes in two species. The colour bar shows the scaled expression level. [Color figure can be viewed at wileyonlinelibrary.com]

these cell types in each species. In Figure 5e, the shared marker gene of *TraesCS7A03G605700* was highly expressed in the endodermis of the wheat (CS) and rice (Nip and 93-11); one *TaRpl10a-1* (*TraesC3B03G1008200*) gene were highly transcribed in the meristem of the wheat (CS) and rice (ZH11). Expression patterns of two shared marker genes in cortex, one in endodermis and three in the epidermis of two species were also plotted by t-SNE (Figure 6). So, data mining of scRNA-seq enabled us to find more information about functional similarity and differences from the cell type to the gene level.

In addition, we identified the highly DEGs, summarized divergent genes with fold change over 5, and their expression heat map showed obviously species-related expression (Table S11, Figure 7a,b). Result, in Figure 7a, the number of genes in epidermis, root hair, stele and xylem are 271, 288, 267 and 275, respectively; in Figure 7b, the number of genes in non-hair, cortex, endodermis, xylem, phloem and root hair is 289, 286, 284, 278 and 314, respectively. Then, we performed GO enrichment of these genes in divergent cell types of two species (Figures 7c,d; Figure S8). For example, ethylene-activated signalling pathway and response to jasmonic acid pathway were accordingly enriched in epidermis of rice (Nip and 93-11) and root hair of wheat (CS) (Figure 7c,d).

Importantly, we found genes encoding *NAC transcription factor 29-like* (*NAC29L*) and protein *PHR1-LIKE 3-like* (*PHR1-L3L*) were highly expressed in wheat (CS) epidermis, and *ethylene-responsive transcription factor 4b* (*ERF4b*), *ethylene transcription factor 4* (*ERF4*) enriched in the ethylene activation pathway were abundantly accumulated in rice (Nip and 93-11) epidermis (Figure 7a); in root hair, *NAC29L* enriched in response to jasmonic acid term, *G-box-binding factor 4-like* (*GBF4L*), *transcription factor RF2a-like* (*RF2aL*) were highly expressed in wheat (CS), and *transcription factor bHLH13-like* (*bHLH13L*), *transcription factor MYC2-like* (*MYC2L*), a predicted protein (*TraesCS7A03G0565100*) belong to *bHLH* family was highly expressed in rice (Nip and 93-11) (Figure 7b). We have listed homologues (> 80% homology) of four transcription factors detected in wheat (CS) epidermis and root hair (Table S11), and the homologues of five transcription factors mentioned above detected in rice (Nip/93-11) did not show high expression in wheat (CS).

3 | Discussion

ScRNA-seq can offer an intensive view of spatiotemporal developmental trajectories at single-cell resolution due to its

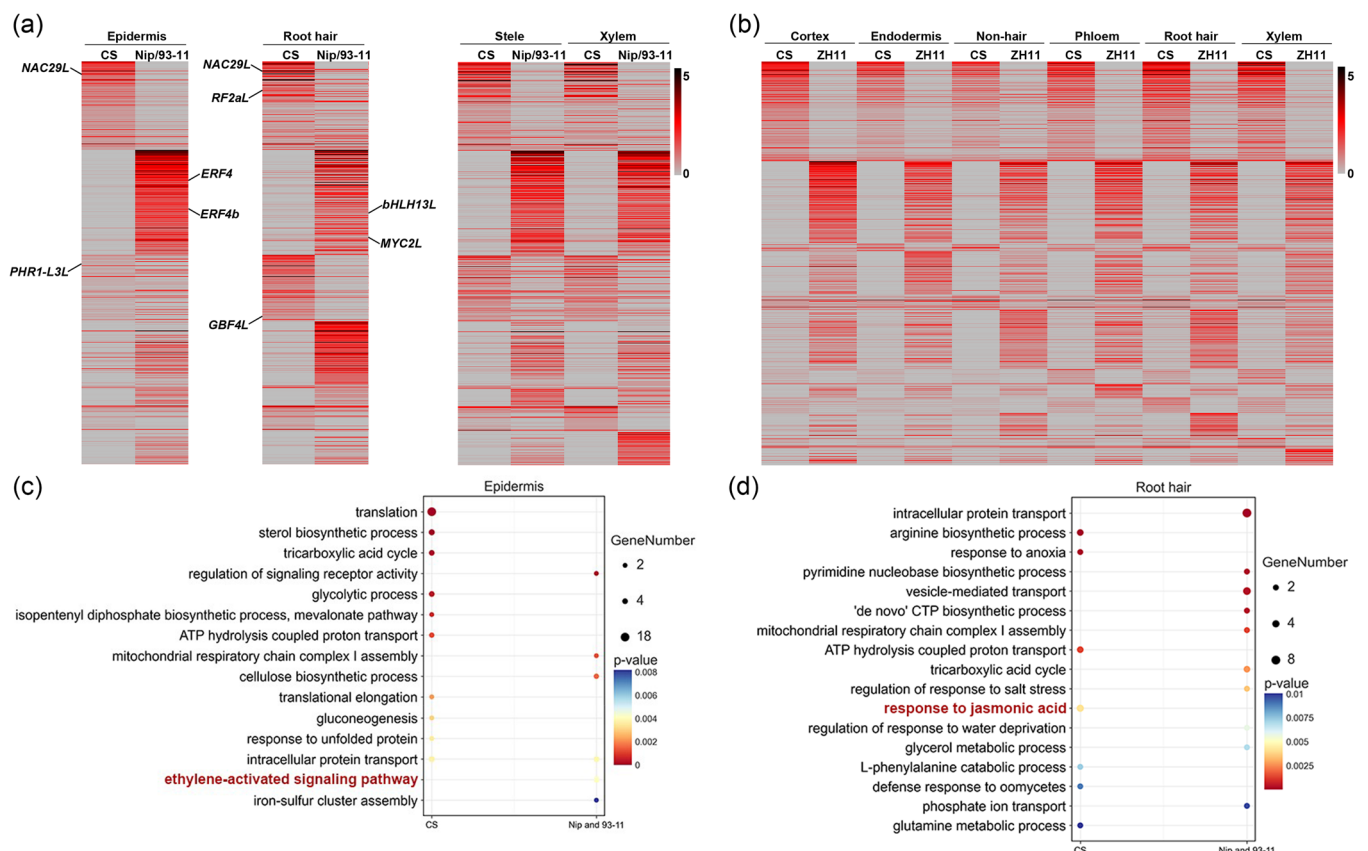


FIGURE 7 | Heatmap showing the expression pattern of divergent genes and GO enrichment of epidermis and root hairs in wheat (CS) and rice (Nip and 93-11). (a, b) Heatmap showing the expression pattern of divergent genes between wheat (CS) and rice (Nip, 93-11) (a) and between wheat (CS) and rice (ZH11) (b). The colour bar shows the scaled expression level. (c, d) GO enrichment of epidermis (c) and root hairs (d) in wheat (CS) and rice (Nip and 93-11). *p* values were showed and the gene number were represented by the size of the filled circles. [Color figure can be viewed at wileyonlinelibrary.com]

unparalleled advantages (Shaw, Tian, and Xu 2021). This study advances the application of scRNA-seq to CS cultivar. Liu et al. (2021) found that the digestion of cell wall had a minor impact on the clustering of rice root tip cells. Furthermore, we focused on specific marker genes related to wheat (CS) root tip cell type, and did not select genes related to stress for analysis. Therefore, we conducted investigation with the protoplasts of wheat (CS) root tips after isolation without consideration of genes induced by isolation process. We collected up to 40 root seedlings to ensure sufficient capture of cells and gene number. According to Figure 1a, through scRNA-seq and clustering analysis of root tips of 4-day-old seedlings, we obtained 19 clusters and annotated 12 cell types. In this study, *t*-SNE plot comprehensively depicted a better display of cell cluster and subcluster (Figure 1a). For analysis and identification of subclusters in Cluster 1, *t*-SNE was also more ideal than UMAP (Figure S2d). To faithfully identify wheat (CS) cell types under circumstances of a lack of available cell-type-specific markers, we applied three strategies to identify cell types, including blasting homologous genes of known cell-type-specific markers in root tips (Table S3; Figure 1c), searching function-annotated genes in other types of reports, and *in situ* assays (Figure 1d). Importantly, *in situ* hybridization was an effective assistant for cell type annotation, which helped us to identify some unassigned cell types. For example, *TraesCS4B03G0998900*, *TraesCS2A03G0222200* and *TaPIP2-6* were highly and specifically expressed in epidermis,

non-hair and root hair cell types (Figure 1d). Finally, we identified most major cell types of the wheat (CS) root tip, such as the cortex, endodermis and epidermis (Figure 1a). Cell types of SCN, TEs and FCs of xylem and phloem, with small cell percentages, were also included (Figure 1a). Therefore, scRNA-seq with incomparable value successfully revealed the transcriptome heterogeneity of cells and the composition of cell types of wheat (CS).

The capture of terminal and intermediate states of cells during the dynamics of differentiation provides a completely new vision for understanding the cellular developmental progressions. Pseudotime analysis enables the arrangement of captured individual cells over developmental time, allowing us to observe continuous differentiation trajectories. In Figure 2a,b, we found that cells of the SCN (Cluster 9), proximal meristem (Cluster 7) and meristemand (Cluster 12) were successively arranged over pseudotime. In Figure 2f, the highly variable genes fell into four modules, and we speculated that the SCN cells from pre-branch differentiated into meristem in branch 1 and proximal meristem in branch 2 after self-renewal in this dynamic process. Consistently, three cell-type-specific markers of three cell types (*TraesCS2B03G0976900*, *TraesCS3B03G1129700*, *TaH3.2*) were expressed at the beginning of the pre-branch and two distinct orientation branches accordingly (Figures 2c-e). Taken together, single-cell atlas helped to achieve pseudotime analysis

which can illustrate the differentiation trajectory and cell fate determination of the SCN, proximal meristem and meristem.

AQPs, which can observably alter the water permeability of cell membranes, demonstrating a critical role in water transportation (Maurel et al. 2002; Javot 2002; Byrt et al. 2017). We noted that *TaTIP1;1*, *TaPIP1;2* and *TaPIP2;1* were expressed in all cell tissues except for root hair (Figures 3a,b,d), indicating the crucial role of cowork by *TaTIP1;1*, *TaPIP1;2* and *TaPIP2;1* in the absorption of water in wheat (CS) root tips. Interestingly, genes of *TaTIP1;5* were detected in all tissues except for TEs (Figures 3a–c), especially six *TaTIP1;5* genes in root hair (Figure 3a,b), which may be an important factor in distinguishing root hair and TEs of xylem from other tissues. The main organ of plant water uptake from the environment is the root, and the main region is the root hair, through which water flow across, in turn, into the epidermis, exodermis, cortex, endodermis, pericycle, xylem parenchyma cells, and finally the vessels (Steudle and Peterson 1998). We found that AQPs were more abundant in root hair, non-hair and cortex than in the endodermis and xylem, so it was speculated that the regulation of water transportation from the root hair of outermost tissue to the xylem of inner tissue was more and more sophisticated, so that the water content of each cell type in the root tips remained within the value required to maintain their respective functions.

Allopolyploidization plays a crucial role in the evolution of vascular plants, possibly more important than any other evolutionary process (Feldman and Levy 2005, 2009). Hexploid wheat undergoes allopolyploidization process and therefore own A, B, and D subgenomes. Allopolyploid plants exist genomic asymmetry and wheat can be a research model (Feldman et al. 2012). Here, we analyzed the asymmetric gene transcription of allohexaploid wheat (CS) root tips at single-cell resolution, and found that the asymmetric gene expression ratio was lower in the cortex, epidermis, stele, xylem, phloem, root hair and meristem, while SCN showed a higher gene unbalanced expression (Figure 4c,d), which were consistent with the research of Zhang et al. (2023). Intriguingly, the enrichment of KEGG in CS and AK58 in SCN illustrated pathway differences in two cultivars at single cell level (Figures 4g,h). However, the higher ratio of gene unbalanced expression in endodermis and non-hair tissues (Figure 4d) in this study were different from the research of Zhang et al. (2023). Furthermore, the minimum ratio of dominant to suppressed gene in A, B, D subgenomes of CS (0.65, 0.65 and 0.85) (Figure 4f) were all higher than those (0.42, 0.45 and 0.71) of AK58 (Zhang et al. 2023). According to Zhang et al. (2023), cell tissues with a higher percentage of asymmetric transcription genes, such as SCN and root border cells, the proportion of almost seven types of genes (A dominant, A suppressed, B dominant, B suppressed, D dominant, D suppressed, central) were higher than that in other tissues. While in this work, the main reason for the higher percentage of asymmetric transcription genes in SCN, endodermis and non-hair was caused by the higher percentage of unbalanced expression in dominant genes from subgenomes (Figure 4d,e).

In the interspecies comparison, the average expression of three copies from three subgenomes of wheat (CS) were used, then one-to-one homologous gene pairs were selected. The cortex

was relatively highly correlated in wheat (CS) and rice (Nip and 93-11) (Figure 5c). In terms of conservation, the cortex of rice (Nip and 93-11) demonstrated a high degree of similarity to the cortex of *Arabidopsis* (Liu et al. 2021). Therefore, the cortex was presumably more conserved in the three species than in other cell types. Conserved marker genes with known functions, such as *TaRpl10a-1* expressed in the meristem of wheat (CS) and rice (ZH11) (Figure 5f), providing a fresh way to further investigate the molecular mechanism relevant to the functions of conserved cell types. In addition, expression of divergent genes (Table S11) and their GO analysis (Figure 7a–d) in divergent cell types of two species could contribute to reveal the functional and morphological differences in root of two species. The expression of transcription factors *NAC29L*, *PHR1-L3L3*, *REFs*, *GBF4L*, *bHLHs* and pathway of response to ethylene and jasmonic acid in the epidermis and root hairs of two species will help to reveal different patterns of epidermal differentiation into root hairs. Currently, only reports from Chen et al. (2020) and Guan et al. (2014) indicated that *bHLH95* and *MYB2* were associated with the development of root hairs. We have shown homologous genes of transcription factors specific to wheat (CS) epidermis and root hair in Table S1, which share over 80% similarity with target factors. All transcription factors may be involved in the morphological difference between the epidermis and root hair of wheat (CS) and rice (Nip and 93-11), such as *ERF4s* related to ethylene-activated signalling pathway and *NAC29L* response to jasmonic acid pathway.

Compared to the snRNA-seq used in transcriptional landscape of root tips in AK58 cultivar (Zhang et al. 2023), scRNA-seq can distinguish closely related cell identities which snRNA-seq frequently cannot achieve (Guillotin et al. 2023). Notably, the epidermis was identified as a separate cell cluster in CS rather than being clustered and annotated together with the cortex or root hairs in AK58. In parallel, CS-dependent novel specific markers of cell types different from AK58 were produced through scRNA-seq. Additionally, the novel findings also included higher asymmetric transcription ratios in endodermis and non-hair tissues, and the increased proportion of dominant genes in three subgenomes accounting for higher asymmetric transcription ratios of SCN, endodermis, non-hair cells in CS, which were different with AK58. Lastly, in the inter-species comparison of wheat (CS) and rice (Nip and 93-11, ZH11), we visualized the expression pattern of conserved markers of highly correlated cell types, and performed the GO function enrichment of differentially expressed genes of divergent cell types in two species, which were not showed in AK58.

We comprehensively characterized the wheat (CS) root developmental programme by the disruptive technology of scRNA-seq. The analysis of specific cell types and novel cell type marker genes was an important extended application of scRNA-seq in CS cultivar of allohexaploid wheat. The development process of the SCN, proximal meristem and meristems illustrated by reconstruction of the differentiation trajectory, the plotted gene expression patterns of water transportation in different cell tissues, and cell-type-specific subgenomes asymmetric transcription could promote to decode important regulatory factors of root tip development at the molecular level. Additionally, the comparative analysis of cell type and gene expression signatures between wheat (CS) and rice (Nip and

93-11, ZH11) could provide a valuable resource for the identification of key genes and their functions in conserved and divergent evolutionary relationships.

4 | Methods

4.1 | Preparation of Wheat (CS) Samples and Protoplast Isolation

The seeds of wheat (CS) were soaked for approximately 12 h and then cultured on filter paper soaked with water. They were grown in a chamber with 12 h light (300 $\mu\text{M}/\text{m}^2/\text{s}$) and 12 h dark cycle at 22°C. After 4 days, root tips of approximately 1 cm of 40 wheat (CS) seedlings were collected. The wheat (CS) root tips were collected and placed in RNase-free enzyme solution (20 mM MES (pH = 5.7), 20 mM KCl, 8% D-mannitol, 2% cellulase R-10, 1% pectinase, 0.4% macerozyme R-10, 0.02 M CaCl₂, 0.1% BSA), and then the mixture was incubated for 2 h in a shaker (room temperature; 90 rpm/min). The protoplasts were filtered twice through 40 μm cell strainers and washed three times with washing solution (20 mM MES (pH = 5.7), 20 mM KCl, 0.1% BSA, 0.4 M D-mannitol). After centrifugation, the supernatant was removed and the protoplasts were resuspended in an 8% D-mannitol solution. Protoplast viability was determined by trypan blue staining. Then, they were adjusted to a concentration of 1000 cells μl^{-1} .

4.2 | ScRNA-Seq Library Construction and Sequencing

After protoplast isolation, wheat (CS) root cells were immediately loaded on a 10 \times Chromium Single Cell Instrument (10 \times Genomics, Pleasanton) to generate single-cell GEMs, and library construction was performed using the Chromium Single Cell 3' Gel Bead and Library Kit v3. An Agilent 2100 Bioanalyzer was used for quantification of the DNA library. Then, the library was sequenced by an Illumina HiSeq2000 sequencer (Shanghai OE Biotech, China).

4.3 | Raw Data Processing, Cell Clustering, and Analysis of DEGs and Marker Genes

The Cell Ranger software pipeline (Version 5.0.0) was used to demultiplex cellular barcodes, map reads to the reference genome and transcriptome using the STAR aligner, and downsample reads to generate normalized aggregate data, which produced a matrix of gene counts versus cells. The genome and GTF annotation information of CS, excluding the organelle genome, was downloaded from URG1 (<https://wheaturgi.versailles.inra.fr/Seq-Repository>). The unique molecular identifier (UMI) count matrix was processed by the R package Seurat (Version 3.1.1) (Butler et al. 2018). To remove low-quality cells and likely multiplet captures, cells with UMI/gene numbers out of the limit of mean value \pm twofold of standard deviations were filtered out. We also applied the DoubletFinder package (Version 2.0.2) (Mcginnis, Murrow, and Gartner 2019) to identify potential doublets. Next, wheat (CS) single cells were included in downstream analyses. To obtain the normalized

count, library size normalization was conducted by the NormalizeData function (LogNormalize method, scaling factor of 10,000 by default) in Seurat (Butler et al. 2018). According to the accession numbers of NC_002762 (Ogihara et al. 2002) and NC_036024 (Cui et al. 2009), the sequences of mitochondrial and chloroplast genes were downloaded from NCBI, respectively. Then they were merged with the wheat genome to calculate the percentage of mitochondrial and chloroplast genes per cell. To identify the top variable genes, the method described by Macosko et al. (2015) was carried out. The most variable genes across single cells were detected with the FindVariableGenes function (mean.function = FastExpMean, dispersion.function = FastLogVMR) in Seurat (Butler et al. 2018). To reduce the dimensionality, PCA was performed with the RunPCA function in Seurat (30 principal components) (Butler et al. 2018). According to the gene expression profile, clustering was performed to cluster cells using the FindClusters function in Seurat (Butler et al. 2018). A two-dimensional t-SNE algorithm with the RunTSNE function in Seurat (Butler et al. 2018) was used for the visualization of cells. The FindAllMarkers function (test.use = bimod) in Seurat (Butler et al. 2018) was used to identify marker genes in each cluster, and for a given cluster, FindAllMarkers identified positive markers compared with all other cells. To infer the cell of origin of each of the single cells and identify cell types, the R package SingleR (Aran et al. 2019) was applied.

DEGs were identified using the FindMarkers function (test.use = MAST) in Seurat (Butler et al. 2018) with a threshold of $p < 0.05$ and $|\log_2\text{foldchange}| > 1.5$ for significant differential expression. GO enrichment and KEGG pathway enrichment analyses of DEGs were performed using R based on the hypergeometric distribution. Regarding the background of GO and KEGG, we used diamond (v0.9.7) software to blast the wheat genome sequence with plant genome database of GO (<http://geneontology.org/>) and KEGG (<http://www.genome.jp/kegg/>). Then, we selected enrichment with an e value threshold of $< 1e -5$ and screened for proteins with the highest sequence similarity. Finally, we obtained functional enrichment of wheat genes and organized them into GO and KEGG background databases for subsequent analysis.

4.4 | Toluidine Blue Staining of Paraffin Sections

Here, 1-cm root tips were fixed in formaldehyde acetic acid (FAA) solution, which consisted of 50% ethanol, 5% formaldehyde, 5% acetic acid, and 5% glycerol. Next, the root tips were dehydrated through ethanol with concentration gradients and HistoClear and cut into paraffin sections. After staining with 0.01% toluidine blue, sections were deparaffinized and dehydrated. Then, staining was performed again for 90 s, with steps of washing in distilled water, dehydrating through ethanol with concentration gradients and sealing, and the sections were observed under a microscope.

4.5 | In Situ hybridization

We used T7 RNA polymerase to synthesize the probe of cell-type-specific markers, and the subsequent hybridization steps

were performed according to Liu et al. (2021) and Zhang et al. (2021). Briefly, paraffin sections of wheat (CS) root tips were subjected to dewaxing, dehydration, proteinase K treatment, probe hybridization, washing, blocking and antibody incubation. Then, NBT/BCIP reagent was used for the detection of hybridization signals. The reagents used above were all produced by Roche. The primers used were shown in Table S12.

4.6 | GO Enrichment Analysis

The GO enrichment analysis was implemented by AgriGO-v2 (Tian et al. 2017). The annotation of pathway enrichment was carried out for genes with high statistical significance, which included cluster-enriched genes, gene modules of pseudotime analysis and conserved, divergent genes of cell types between wheat (CS) and rice (Nip, 93-11 and ZH11).

4.7 | Pseudotime Trajectory Analysis

Monocle 2 (v2.9.0) (Trapnell et al. 2014) was applied for pseudotime analysis to infer the cell differentiation trajectory and the cell fate determination of the SCN and meristem. The subset of raw data of Clusters 7, 9 and 12 were extracted for subsequent analysis. First, we used the dispersion table function to calculate the variance in the expression of each gene and chose variable genes with average expression level information to define a developmental trajectory. Then, the reduceDimension function, max_components = 2, reducion_Method = “DDRTree” was applied for dimension reduction clustering analysis. Finally, the differentiation trajectory was inferred by the “orderCells” function. The detailed process was described by Liu et al. (2021).

4.8 | Asymmetric Gene Expression in Subgenome of Wheat (CS)

The asymmetric transcription analysis was performed as described previously (Zhang et al. 2023). Briefly, according to the triads of the A, B and D subgenomes of allohexaploid wheat, we extracted triads of homoeolog and standardized their relative expression levels to make the sum of the homoeolog gene expression in each triad was 1. Then, the triads were identified into 7 categories (Balance, A. dominant, B. dominant, D. dominant, A. suppressed, B. suppressed, and D. suppressed) and results were visualized using R package ggtern v3.3.5.

4.9 | Interspecies Comparison of Wheat (CS) and Rice (Nip and 93-11, ZH11) Data Sets

From the reports of Liu et al. (2021) and Zhang et al. (2021), we obtained the scRNA-seq data sets of rice (Nip and 93-11, ZH11). First, the protein sequences of wheat (CS) and rice (Nip and 93-11, ZH11) were compared with BLASTP (e value < 1e-5) according to OrthoMCL (Li, Stoeckert, and Roos 2003). The average expression of three copies from each subgenome of wheat were used to compare the expression levels of one-to-one homologues, and one-to-one homologous gene pairs were

selected for subsequent analysis. Then, based on the homologous gene pairs, genes in the rice project were replaced with wheat (CS) homologous genes, while genes without homologous genes were removed. Marker genes as well as DEGs between individual clusters were determined by the FindMarkers function in Seurat (Butler et al. 2018), with a p value < 0.05 and |log₂fold change| > 1.5. There were 15 367, 15 263 and 15 388 one-to-one homologous gene pairs of wheat (CS) and rice (Nip and 93-11), wheat (CS) and rice (ZH11), respectively.

Through “FindConservedMarkers” we identified the conserved and species-specific genes between wheat (CS) and rice (Nip and 93-11, ZH11) of relatively highly correlated cell types. DEGs of divergent cell types were identified through the FindMarkers function (test.use = MAST) in Seurat. DEGs with fold change over 5 in divergent cell types were identified as the divergent genes. The GO enrichment analysis of divergent genes was performed as mentioned above.

Acknowledgements

This work was supported by Xinjiang Major Science and Technology projects (Research, development, and demonstration of key technologies for the green control of major pests on special and superiority crops in Xinjiang, 2023A02009). Li Gao was supported by the Xinjiang 2+5 Key Talent Plan Project.

Conflicts of Interest

The authors declare no conflicts of interest.

Data Availability Statement

The scRNA-seq raw data of Illumina sequencing have been deposited in the NCBI GEO with the accession number GSE222422. All the other data and materials are available from the corresponding authors upon request.

References

- Aran, D., A. P. Looney, L. Liu, et al. 2019. “Reference-Based Analysis of Lung Single-Cell Sequencing Reveals a Transitional Profibrotic Macrophage.” *Nature Immunology* 20: 163–172.
- Avci, U., H. Earl Petzold, I. O. Ismail, E. P. Beers, and C. H. Haigler. 2008. “Cysteine Proteases XCP1 and XCP2 Aid Micro-Autolysis Within the Intact Central Vacuole During Xylogenesis in *Arabidopsis* Roots.” *Plant Journal* 56: 303–315.
- Barros, J., H. Serk, I. Granlund, and E. Pesquet. 2015. “The Cell Biology of Lignification in Higher Plants.” *Annals of Botany* 115: 1053–1074.
- Beneteau, J., D. Renard, L. Marché, et al. 2010. “Binding Properties of the N-Acetylglucosamine and High-Mannose N-Glycan PP2-A1 Phloem Lectin in *Arabidopsis*.” *Plant Physiology* 153: 1345–1361.
- Butler, A., P. Hoffman, P. Smibert, E. Papalexi, and R. Satija. 2018. “Integrating Single-Cell Transcriptomic Data Across Different Conditions, Technologies, and Species.” *Nature Biotechnology* 36: 411–420.
- Byrt, C. S., M. Zhao, M. Kourghi, et al. 2017. “Non-Selective Cation Channel Activity of Aquaporin AtPIP2;1 Regulated by Ca²⁺ and pH.” *Plant, Cell & Environment* 40: 802–815.
- Chen, Y., D. Su, J. Li, et al. 2020. “Overexpression of *bHLH95*, a Basic Helix-Loop-Helix Transcription Factor Family Member, Impacts Trichome Formation via Regulating Gibberellin Biosynthesis in Tomato.” *Journal of Experimental Botany* 71: 3450–3462.
- Choi, D. W., J. Y. Song, Y. M. Kwon, and S. G. Kim. 1996. “Characterization of a cDNA Encoding a Proline-Rich 14 kDa Protein in

- Developing Cortical Cells of the Roots of Bean (*Phaseolus vulgaris*) Seedlings." *Plant Molecular Biology* 30: 973–982.
- Cui, P., H. Liu, Q. Lin, et al. 2009. "A Complete Mitochondrial Genome of Wheat (*Triticum aestivum* cv. Chinese Yumai), and Fast Evolving Mitochondrial Genes in Higher Plants." *Journal of Genetics* 88: 299–307.
- Denyer, T., X. Ma, S. Klesen, E. Scacchi, K. Nieselt, and M. C. P. Timmermans. 2019. "Spatiotemporal Developmental Trajectories in the *Arabidopsis* Root Revealed Using High Throughput Single-Cell RNA Sequencing." *Developmental Cell* 48: 840–852.e5.
- Dinant, S., A. M. Clark, Y. Zhu, et al. 2003. "Diversity of the Superfamily of Phloem Lectins (Phloem Protein 2) in Angiosperms." *Plant Physiology* 131: 114–128.
- Ding, L., N. Uehlein, R. Kaldenhoff, S. Guo, Y. Zhu, and L. Kai. 2019. "Aquaporin PIP2;1 Affects Water Transport and Root Growth in Rice (*Oryza sativa* L.)." *Plant Physiology and Biochemistry* 139: 152–160.
- Dubey, S. M., N. B. C. Serre, D. Oulehlová, P. Vittal, and M. Fendrych. 2021. "No Time for Transcription-Rapid Auxin Responses in Plants." *Cold Spring Harbor Perspectives in Biology* 13: a039891.
- Efroni, I., and K. D. Birnbaum. 2016. "The Potential of Single-Cell Profiling in Plants." *Genome Biology* 17: 65.
- Feldman, M., and A. A. Levy. 2005. "Allopolyploidy—A Shaping Force in the Evolution of Wheat Genomes." *Cytogenetic and Genome Research* 109: 250–258.
- Feldman, M., and A. A. Levy. 2009. "Genome Evolution in Allopolyploid Wheat—a Revolutionary Reprogramming Followed by Gradual Changes." *Journal of Genetics and Genomics* 36: 511–518.
- Feldman, M., A. A. Levy, T. Fahima, and A. Korol. 2012. "Genomic Asymmetry in Allopolyploid Plants: Wheat as a Model." *Journal of Experimental Botany* 63: 5045–5059.
- Fetter, K., V. Van Wilder, M. Moshelion, and F. Chaumont. 2004. "Interactions Between Plasma Membrane Aquaporins Modulate Their Water Channel Activity." *Plant Cell* 16: 215–228.
- Funk, V., B. Kositsup, C. Zhao, and E. P. Beers. 2002. "The *Arabidopsis* Xylem Peptidase XCP1 Is a Tracheary Element Vacuolar Protein That May Be a Papain Ortholog." *Plant Physiology* 128: 84–94.
- Guan, X., M. Pang, G. Nah, et al. 2014. "miR828 and miR858 Regulate Homoeologous *MYB2* Gene Functions in *Arabidopsis* Trichome and Cotton Fibre Development." *Nature Communications* 5: 3050.
- Guillotin, B., R. Rahni, M. Passalacqua, et al. 2023. "A Pan-Grass Transcriptome Reveals Patterns of Cellular Divergence in Crops." *Nature* 617: 785–791.
- Hamanaka, R. B., A. Glasauer, P. Hoover, et al. 2013. "Mitochondrial Reactive Oxygen Species Promote Epidermal Differentiation and Hair Follicle Development." *Science Signaling* 6: 8.
- Horie, T., T. Kaneko, G. Sugimoto, et al. 2011. "Mechanisms of Water Transport Mediated by Pip Aquaporins and Their Regulation via Phosphorylation Events Under Salinity Stress in Barley Roots." *Plant and Cell Physiology* 52: 663–675.
- Hoskins, J. A. 1984. "The Occurrence, Metabolism and Toxicity of Cinnamic Acid and Related Compounds." *Journal of Applied Toxicology* 4: 283–292.
- Javot, H. 2002. "The Role of Aquaporins in Root Water Uptake." *Annals of Botany* 90: 301–313.
- Jean-Baptiste, K., J. L. McFaline-Figueroa, C. M. Alexandre, et al. 2019. "Dynamics of Gene Expression in Single Root Cells of *Arabidopsis thaliana*." *Plant Cell* 31: 993–1011.
- Lee, Y., M. C. Rubio, J. Alassimone, and N. Geldner. 2013. "A Mechanism for Localized Lignin Deposition in the Endodermis." *Cell* 153: 402–412.
- Li, H., X. Dai, X. Huang, et al. 2021. "Single-Cell RNA Sequencing Reveals a High-Resolution Cell Atlas of Xylem in *Populus*." *Journal of Integrative Plant Biology* 63: 1906–1921.
- Li, L., C. J. Stoeckert, Jr., and D. S. Roos. 2003. "OrthoMCL: Identification of Ortholog Groups for Eukaryotic Genomes." *Genome Research* 13: 2178–2189.
- Li, L., Y. Xu, Y. Ren, et al. 2019. "Comparative Proteomic Analysis Provides Insights Into the Regulatory Mechanisms of Wheat Primary Root Growth." *Scientific Reports* 9: 11741.
- Li, X., X. Zhang, S. Gao, et al. 2022. "Single-Cell RNA Sequencing Reveals the Landscape of Maize Root Tips and Assists in Identification of Cell Type-Specific Nitrate-Response Genes." *Crop Journal* 10: 1589–1600.
- Liu, Q., Z. Liang, D. Feng, et al. 2021. "Transcriptional Landscape of Rice Roots at the Single-Cell Resolution." *Molecular Plant* 14: 384–394.
- Liu, Z., Y. Zhou, J. Guo, et al. 2020. "Global Dynamic Molecular Profiling of Stomatal Lineage Cell Development by Single-Cell RNA Sequencing." *Molecular Plant* 13: 1178–1193.
- Macosko, E. Z., A. Basu, R. Satija, et al. 2015. "Highly Parallel Genome-Wide Expression Profiling of Individual Cells Using Nanoliter Droplets." *Cell* 161: 1202–1214.
- Madrid-Espinoza, J., N. Brunel-Saldias, F. P. Guerra, A. Gutiérrez, and A. Del-Pozo. 2018. "Genome-Wide Identification and Transcriptional Regulation of Aquaporin Genes in Bread Wheat (*Triticum aestivum* L.) Under Water Stress." *Genes* 9: 497.
- Malinska, D., A. P. Kudin, M. Bejtka, and W. S. Kunz. 2012. "Changes in Mitochondrial Reactive Oxygen Species Synthesis During Differentiation of Skeletal Muscle Cells." *Mitochondrion* 12: 144–148.
- Maurel, C., H. Javot, V. Lauvergeat, et al. 2002. "Molecular Physiology of Aquaporins in Plants." *International Review Review of Cytology Cytology* 215: 105–148.
- McGinnis, C. S., L. M. Murrow, and Z. J. Gartner. 2019. "Doubletfinder: Doublet Detection in Single-Cell RNA Sequencing Data Using Artificial Nearest Neighbors." *Cell Systems* 8: 329–337.e4.
- Mockaitis, K., and M. Estelle. 2008. "Auxin Receptors and Plant Development: A New Signaling Paradigm." *Annual Review of Cell and Developmental Biology* 24: 55–80.
- Nelms, B., and V. Walbot. 2019. "Defining the Developmental Program Leading to Meiosis in Maize." *Science* 364: 52–56.
- Ogihara, Y., K. Isono, T. Kojima, et al. 2002. "Structural Features of a Wheat Plastome as Revealed by Complete Sequencing of Chloroplast DNA." *Molecular Genetics and Genomics* 266: 740–746.
- Oh, E., P. J. Seo, and J. Kim. 2017. "Signaling Peptides and Receptors Coordinating Plant Root Development." *Trends in Plant Science* 23: 337–351.
- Ohashi-Ito, K., and H. Fukuda. 2014. "Xylem." *Current Biology* 24: R1149.
- Ortega-Martínez, O., M. Pernas, R. J. Carol, and L. Dolan. 2007. "Ethylene Modulates Stem Cell Division in the *Arabidopsis thaliana* Root." *Science* 317: 507–510.
- Ortiz-Ramírez, C., B. Guillotin, X. Xu, et al. 2021. "Ground Tissue Circuitry Regulates Organ Complexity in Maize and *Setaria*." *Science* 374: 1247–1252.
- Reyt, G., Z. Chao, P. Flis, et al. 2020. "Uclacyanin Proteins Are Required for Lignified Nanodomain Formation Within Casparyan Strips." *Current Biology* 30: 4103–4111.e6.
- Rich-Griffin, C., A. Stechemesser, J. Finch, E. Lucas, S. Ott, and P. Schäfer. 2020. "Single-Cell Transcriptomics: A High-Resolution Avenue for Plant Functional Genomics." *Trends in Plant Science* 25: 186–197.
- Ryu, K. H., L. Huang, H. M. Kang, and J. Schiefelbein. 2019. "Single-Cell RNA Sequencing Resolves Molecular Relationships Among Individual Plant Cells." *Plant Physiology* 179: 1444–1456.

- Santuari, L., G. F. Sanchez-Perez, M. Luijten, et al. 2016. "The PLETHORA Gene Regulatory Network Guides Growth and Cell Differentiation in *Arabidopsis* Roots." *Plant Cell* 28: 2937–2951.
- Satterlee, J. W., J. Strable, and M. J. Scanlon. 2020. "Plant Stem-Cell Organization and Differentiation at Single-Cell Resolution." *Proceedings of the National Academy of Sciences of the United States of America* 117: 33689–33699.
- Schneider, R., L. Tang, E. R. Lampugnani, et al. 2017. "Two Complementary Mechanisms Underpin Cell Wall Patterning During Xylem Vessel Development." *Plant Cell* 29: 2433–2449.
- Shaw, R., X. Tian, and J. Xu. 2021. "Single-Cell Transcriptome Analysis in Plants: Advances and Challenges." *Molecular Plant* 14: 115–126.
- Shulse, C. N., B. J. Cole, D. Ciobanu, et al. 2019. "High-Throughput Single-Cell Transcriptome Profiling of Plant Cell Types." *Cell Reports* 27: 2241–2247.e4.
- Steudle, E., and C. A. Peterson. 1998. "How Does Water Get Through Roots?" *Journal of Experimental Botany* 49: 775–788.
- Tadesse, W., M. Sanchez-Garcia, S. G. Assefa, A. Amri, and M. Baum. 2019. "Genetic Gains in Wheat Breeding and Its Role in Feeding the World." *Crop Breeding, Genetics and Genomics* 1, no. 1–28: e190005.
- Tanaka, K., K. Murata, M. Yamazaki, K. Onosato, A. Miyao, and H. Hirochika. 2003. "Three Distinct Rice Cellulose Synthase Catalytic Subunit Genes Required for Cellulose Synthesis in the Secondary Wall." *Plant Physiology* 133: 73–83.
- Tian, T., Y. Liu, H. Yan, et al. 2017. "agriGO v2.0: A GO Analysis Toolkit for the Agricultural Community, 2017 Update." *Nucleic Acids Research* 45: W122–W129.
- Trapnell, C., D. Cacchiarelli, J. Grimsby, et al. 2014. "The Dynamics and Regulators of Cell Fate Decisions Are Revealed by Pseudotemporal Ordering of Single Cells." *Nature Biotechnology* 32: 381–386.
- Tsukagoshi, H., W. Busch, and P. N. Benfey. 2010. "Transcriptional Regulation of ROS Controls Transition From Proliferation to Differentiation in the Root." *Cell* 143: 606–616.
- Turner, S., P. Gallois, and D. Brown. 2007. "Tracheary Element Differentiation." *Annual Review of Plant Biology* 58: 407–433.
- Wang, D., S. Yuan, L. Yin, et al. 2012. "A Missense Mutation in the Transmembrane Domain of CES49 Affects Cell Wall Biosynthesis and Plant Growth in Rice." *Plant Science* 196: 117–124.
- Wang, G. F., Y. He, R. Strauch, et al. 2015. "Maize Homologs of Hydroxycinnamoyltransferase, a Key Enzyme in Lignin Biosynthesis, Bind the Nucleotide Binding Leucine-Rich Repeat RP1 Proteins to Modulate the Defense Response." *Plant Physiology* 169: 2230–2243.
- Wang, Y., Q. Huan, K. Li, and W. Qian. 2021. "Single-Cell Transcriptome Atlas of the Leaf and Root of Rice Seedlings." *Journal of Genetics and Genomics* 48: 881–898.
- Yamada, S., K. Nabe, N. Izuo, K. Nakamichi, and I. Chibata. 1981. "Production of L-Phenylalanine From Trans-Cinnamic Acid With *Rhodotorula glutinis* Containing L-Phenylalanine Ammonia-Lyase Activity." *Applied and Environmental Microbiology* 42: 773–778.
- Yamaguchi, M., N. Mitsuda, M. Ohtani, M. Ohme-Takagi, K. Kato, and T. Demura. 2011. "VASCULAR-RELATED NAC-DOMAIN7 Directly Regulates the Expression of a Broad Range of Genes for Xylem Vessel Formation." *Plant Journal* 66: 579–590.
- Zeng, J., Z. Dong, H. Wu, Z. Tian, and Z. Zhao. 2017. "Redox Regulation of Plant Stem Cell Fate." *EMBO Journal* 36: 2844–2855.
- Zhang, L., C. He, Y. Lai, et al. 2023. "Asymmetric Gene Expression and Cell-Type-Specific Regulatory Networks in the Root of Bread Wheat Revealed By Single-Cell Multiomics Analysis." *Genome Biology* 24: 65.
- Zhang, T. Q., Y. Chen, Y. Liu, W. H. Lin, and J. W. Wang. 2021. "Single-Cell Transcriptome Atlas and Chromatin Accessibility Landscape Reveal Differentiation Trajectories in the Rice Root." *Nature Communications* 12: 2053.
- Zhang, T. Q., Y. Chen, and J. W. Wang. 2021. "A Single-Cell Analysis of the *Arabidopsis* Vegetative Shoot Apex." *Developmental Cell* 56: 1056–1074.e8.
- Zhang, T. Q., Z. G. Xu, G. D. Shang, and J. W. Wang. 2019. "A Single-Cell RNA Sequencing Profiles the Developmental Landscape of *Arabidopsis* Root." *Molecular Plant* 12: 648–660.
- Zhuang, Y., D. Zuo, Y. Tao, H. Cai, and L. Li. 2020. "Laccase 3-based Extracellular Domain Provides Possible Positional Information for Directing Caspary Strip Formation in *Arabidopsis*." *Proceedings of the National Academy of Sciences of the United States of America* 117: 202005429.
- Zong, J., L. Wang, L. Zhu, et al. 2022. "A Rice Single Cell Transcriptomic Atlas Defines the Developmental Trajectories of Rice Floret and Inflorescence Meristems." *New Phytologist* 234: 494–512.

Supporting Information

Additional supporting information can be found online in the Supporting Information section.